

Neutron diffraction study of crystal structure and antiferromagnetic order in $\text{Sr}_2\text{CoO}_2\text{X}_2$ ($X=\text{Cl}, \text{Br}$)

Christopher S. Knee* and Mark T. Weller

Inorganic Materials Group, School of Chemistry, University of Southampton, Southampton, SO17 1BJ, United Kingdom

(Received 7 January 2004; revised manuscript received 7 June 2004; published 15 October 2004)

The crystal and magnetic structures of polycrystalline samples of the cobalt oxyhalides $\text{Sr}_2\text{CoO}_2\text{X}_2$, $X=\text{Cl}$ and Br , have been studied using variable temperature neutron diffraction. The materials are isostructural with the K_2NiF_4 -type square lattice Heisenberg antiferromagnet $\text{Sr}_2\text{CuO}_2\text{Cl}_2$ and contain two-dimensional CoO_2 sheets separated along z by double rocksalt SrX layers. Both materials exhibit magnetic Bragg scattering indicative of long range antiferromagnetic order at $T \leq 20$ K. The thermal evolution of magnetic reflections has allowed a $T_N=215(10)$ K to be determined for $\text{Sr}_2\text{CoO}_2\text{Cl}_2$. No evidence of a lowering of crystal symmetry at the onset of magnetic order within $\text{Sr}_2\text{CoO}_2\text{Cl}_2$ is found and the crystal structure of both materials in their antiferromagnetically ordered states is well described with $I4/mmm$ symmetry. The coexistence of domains with the La_2CuO_4 -type and La_2NiO_4 -type spin structures is proposed to account for the observed magnetic scattering. The ordered moments of $\text{Sr}_2\text{CoO}_2\text{Cl}_2$ and $\text{Sr}_2\text{CoO}_2\text{Br}_2$ obtained at 20 K and 2 K, respectively, are $3.22(4)\mu_B$ and $3.52(7)\mu_B$ indicating the presence of a significant orbital contribution in these high spin ($S=3/2$) cobalt (II) systems.

DOI: 10.1103/PhysRevB.70.144406

PACS number(s): 75.50.Ee, 75.25.+z, 61.12.Ld

I. INTRODUCTION

The discovery of superconductivity within the copper-oxygen planes of materials such as $\text{La}_{2-x}\text{Sr}_x\text{CuO}_4$ (Ref. 1) and $\text{YBa}_2\text{Cu}_3\text{O}_7$ (Ref. 2) has given renewed impetus to the study of two-dimensional (2D) magnetic systems. In particular the superexchange interactions between the Cu^{2+} ions of the undoped parent phase La_2CuO_4 have been investigated in great detail^{3,4} and the phase is now viewed as a 2D spin- $\frac{1}{2}$ Heisenberg antiferromagnet.⁵ The antiferromagnetic (AF) interactions within the isostructural La_2MO_4 , $M=\text{Ni}$ ($S=1$)^{6,7} and Co ($S=3/2$),⁸ systems have also been the focus of several studies aimed at revealing which factors uniquely allow the lamellar cuprates to support superconductivity. Much of this work has drawn on the theories developed for the classical layered antiferromagnets such as K_2NiF_4 (Ref. 9) and Rb_2CoF_4 (Ref. 10).

An essential feature of many two-dimensional (2D) antiferromagnets is the relative weakness of the interlayer interaction compared with intraplanar metal to metal coupling, with typically $J_{\text{inter}}/J_{\text{intra}} \approx 10^{-3} - 10^{-6}$. Consequently, the onset of long range magnetic order may often be viewed to occur in two dimensions first, with three-dimensional (3D) order following parasitically in the presence of even a weak interlayer coupling. A range of factors including the metal ion environment, possible single ion anisotropy contributions and interlayer interactions, originating from either dipolar or exchange perturbations, lead to a variety of spin structures being adopted. The three common arrangements exhibited by K_2NiF_4 -type materials are summarized in Fig. 1. The importance of the materials crystal structure is exemplified by the magnetism displayed by La_2CoO_4 for which Yamada *et al.*⁸ have observed successive AF transitions. The spin lattice switches from a La_2NiO_4 [Fig. 1(b)] model in the orthorhombic phase to an arrangement which may be represented by the collinear La_2CuO_4 structure [Fig. 1(a)] in its low temperature tetragonal phase.

The related cuprate oxychloride, $\text{Sr}_2\text{CuO}_2\text{Cl}_2$, crystallizes in the ideal K_2NiF_4 $I4/mmm$ structure at room temperature, in contrast to the orthorhombic cell favored by La_2CuO_4 , with chloride ions replacing the apical oxygen ions above and below the CuO_2 sheets. The system adopts a La_2CuO_4 -type spin configuration [Fig. 1(a)] with transition temperatures in the range 250–260 K reported^{11,12} and an ordered copper moment of $0.34(4)\mu_B$ at 10 K has been determined from a single crystal neutron study.¹¹ The compound has been the focus of numerous investigations probing, for example, the spin dynamics,¹³ and the strength of the coupling within the antiferromagnetic sheets.¹⁴ In this context it is desirable to develop new planar systems to further investigate the magnetic interactions within and between the key MO_2 layers. Motivated by this goal we have recently synthesized the cuprate oxide iodides, $\text{Sr}_2\text{CuO}_2\text{I}_2$ and $\text{Sr}_2\text{Cu}_3\text{O}_4\text{I}_2$ (Ref. 15) and the Co(II) materials $\text{Sr}_2\text{CoO}_2\text{X}_2$, $X=\text{Cl}$ and Br .¹⁶ These latter materials are the first transition metal phases isostructural with $\text{Sr}_2\text{CuO}_2\text{Cl}_2$ and are of particular interest as cobalt (II) systems display an electronic configuration similar to the cuprates, with half-occupied $d_{x^2-y^2}$ orbitals, which facilitate in-plane superexchange cou-

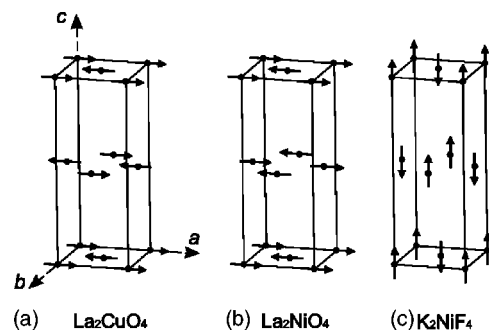


FIG. 1. Commonly observed magnetic structures for K_2NiF_4 -type antiferromagnets.

TABLE I. Structural parameters for $\text{Sr}_2\text{CoO}_2\text{X}_2$ ($X=\text{Cl}$ and Br) determined from the C-Bank of POLARIS. Top lines are refined from data collected at RT, lower lines at 20 K ($X=\text{Cl}$) and 2 K ($X=\text{Br}$). Space group $I4/mmm$. The * represents weight percent $\text{Sr}_2\text{CoO}_2\text{Br}_2$ (93.2%), CoO (1.9%) and SrCO_3 (4.9%).

Atom	Site	$\text{Sr}_2\text{CoO}_2\text{Cl}_2$		* $\text{Sr}_2\text{CoO}_2\text{Br}_2$	
		z	$U_{\text{iso}} \times 100$ (\AA^2)	z	$U_{\text{iso}} \times 100$ (\AA^2)
Sr	(0,0, z) 4e	0.39191(5)	0.79(1)	0.40106(4)	0.84(2)
		0.39165(3)	0.23(1)	0.40047(6)	0.16(2)
Co	(0,0,0) 2a		0.79(4)		0.83(4)
			0.33(2)		0.55(7)
O	(0, $\frac{1}{2}$,0) 4c		0.84(1)		0.84(2)
			0.40(8)		0.57(2)
X	(0,0, z) 4e	0.18087(4)	1.11(8) ^a	0.17769(5)	1.18(9) ^c
		0.18098(2)	0.34(5) ^b	0.17803(7)	0.40(2) ^d
a (\AA)		4.06022(2)		4.08891(7)	
		4.05013(2)		4.07478(5)	
c (\AA)		15.1171(1)		16.4077(4)	
		15.0247(1)		16.2426(3)	
χ^2		1.89		3.95	
		2.46		5.66	
R_{wp} (%)		1.48		2.43	
		1.72		1.77	
R_p (%)		3.16		4.68	
		4.01		3.04	

^a $u_{11}=u_{22}=0.96(2)$, $u_{33}=1.45(4)$.

^b $u_{11}=u_{22}=0.27(1)$, $u_{33}=0.53(3)$.

^c $u_{11}=u_{22}=1.08(2)$, $u_{33}=1.38(4)$.

^d $u_{11}=u_{22}=0.14(2)$, $u_{33}=0.86(4)$.

pling. Herein we present the results of a variable temperature neutron powder diffraction (NPD) investigation that has revealed a transition to long range AF order in both phases. The results are compared with those obtained for $\text{Sr}_2\text{CuO}_2\text{Cl}_2$ and the closely related La_2MO_4 oxides, $M=\text{Cu}$ and Co , to provide further insight into the structural and magnetic characteristics of these planar materials.

II. EXPERIMENT

5 g samples of $\text{Sr}_2\text{CoO}_2\text{X}_2$ ($X=\text{Cl}$ and Br) were synthesised as described previously.¹⁶ Time-of-flight NPD data were then collected using the medium resolution POLARIS diffractometer at the ISIS facility in the UK. The $\text{Sr}_2\text{CoO}_2\text{Cl}_2$ sample was loaded into an air-tight vanadium can in a helium gas atmosphere and data collection performed at RT (295 K), 20 K, 70 K, 120 K, 170 K, 195 K, and 220 K using a closed cycle refrigerator. Further scans were obtained for $\text{Sr}_2\text{CoO}_2\text{Br}_2$ at room temperature and at 2 K inside a cryostat. The diffraction data were analyzed using the Rietveld method¹⁷ and GSAS software package¹⁸ with the structural models reported from the powder x-ray diffraction (PXRD) analyses¹⁶ employed in initial cycles. The higher resolution C-bank data of POLARIS (d -spacing range 0.2–3.2 \AA) were used for the structural refinements while the magnetic struc-

tures of the materials were determined from the wider range (0.5–8.3 \AA) lower resolution A-bank patterns.

III. RESULTS

A. Crystal structure analysis

Refinement of the nuclear structures of the $\text{Sr}_2\text{CoO}_2\text{X}_2$ phases using the variable temperature NPD data confirmed the accuracy of the previously reported models derived from PXD data.¹⁶ The only significant difference was that the NPD data allowed the refinement of anisotropic atomic thermal displacement parameters for the halide sites. This produced an appreciable improvement in the least squares fit and points to some localized displacements of the ions along the c axis. For the $\text{Sr}_2\text{CoO}_2\text{Cl}_2$ refinements a trace level of CoO impurity was apparent while for the $\text{Sr}_2\text{CoO}_2\text{Br}_2$ analyses CoO and SrCO_3 impurities were identified and refined to 1.9 wt. % and 4.9 wt. %, respectively. In the final stages of the refinements the occupancy of each site was permitted to vary and no significant site deficiencies were detected indicating that the impurity levels were too low to impact on the main phase stoichiometry within the detection limits of NPD. Table I summarizes the structural parameters derived from the analysis of NPD data collected at RT, and low temperatures, i.e., 20 K and 2 K for $\text{Sr}_2\text{CoO}_2\text{Cl}_2$ and $\text{Sr}_2\text{CoO}_2\text{Br}_2$,

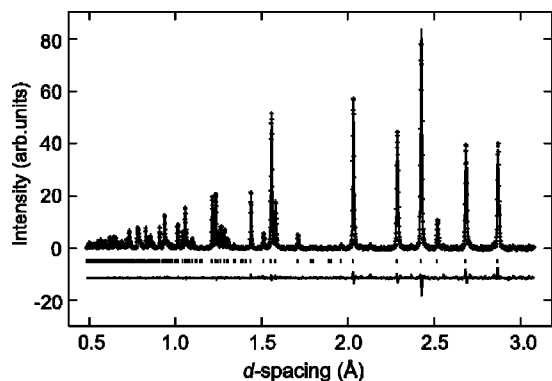


FIG. 2. The NPD pattern obtained for $\text{Sr}_2\text{CoO}_2\text{Cl}_2$ from the POLARIS C-bank at RT. Crosses are observed data, lines are calculated and difference plots. Vertical tick marks indicate the position of allowed reflections for the nuclear structure of $\text{Sr}_2\text{CoO}_2\text{Cl}_2$.

respectively. The profile fit achieved to the RT data of $\text{Sr}_2\text{CoO}_2\text{Cl}_2$ is shown in Fig. 2.

B. Magnetic structure analysis

Additional intense Bragg reflections appeared in the A-bank data sets collected for both materials at low temperatures that could not be accounted for by their nuclear structures. The high d -spacing position of the peaks indicated that they were probably magnetic and this was confirmed by variable temperature scans performed on $\text{Sr}_2\text{CoO}_2\text{Cl}_2$ that showed that the reflections decayed on warming. The main magnetic intensities could be indexed as the (100), (011), (102), and (013) reflections of a magnetic cell related to the nuclear cell by $a_{\text{mag}}=b_{\text{mag}}=\sqrt{2}a_{\text{nuc}}$ and $c_{\text{mag}}=c_{\text{nuc}}$. This behavior is analogous to that of both La_2CuO_4 (Ref. 3) and

$\text{Sr}_2\text{CuO}_2\text{Cl}_2$ (Ref. 11) and, for a collinear magnetic structure, indicates a propagation vector $\mathbf{k}=(\frac{1}{2}, \frac{1}{2}, 0)$.

Analysis proceeded using the magnetic form factor of Co^{2+} (Ref. 19) and the La_2CuO_4 spin model was introduced into the 20 K $\text{Sr}_2\text{CoO}_2\text{Cl}_2$ A-bank refinement. This spin description produced a partial fit to the observed magnetic intensity, however sizeable discrepancies were apparent as, for example, the intensity of the (011) reflection was significantly underestimated. To check for further symmetry allowed spin arrangements the SARAH representational analysis package²⁰ was used and the spin descriptions shown in Fig. 1 were found to be the only structures consistent with $I4/mmm$ crystal symmetry above the magnetic phase transition. The spin arrangement adopted by La_2NiO_4 [Fig. 1(b)] was found to produce a good fit to the (011) peak but, as can be seen from Table II, the (100) is absent for this model. Finally, the K_2NiF_4 structure [Fig. 1(c)] with the Co spins aligned parallel to the c direction was employed to give an improved agreement between the observed and calculated intensities. However the fit was still far from ideal and when the K_2NiF_4 model was introduced into the 2 K A-Bank scan of $\text{Sr}_2\text{CoO}_2\text{Br}_2$ a poor fit to the magnetic intensities was obtained indicating that the spin direction is not along the tetragonal axis within the bromide analogue. Given the close structural similarity between the $X=\text{Cl}$ and $X=\text{Br}$ materials it is unlikely that the spin alignment within the two materials will differ significantly. Therefore, a two phase magnetic model with an initial 50:50 distribution of La_2CuO_4 and La_2NiO_4 spin structures was considered. This two-phase approach resolved the earlier intensity problems obtained when each model was refined on an individual basis and critically resulted in good agreement for both $\text{Sr}_2\text{CoO}_2\text{Cl}_2$ and $\text{Sr}_2\text{CoO}_2\text{Br}_2$ data sets. The size of the moment within each phase was constrained to be equal, and the phase fractions constrained to sum to half that of the nuclear cell (to account

TABLE II. Comparison of calculated and observed magnetic intensities for $\text{Sr}_2\text{CoO}_2\text{X}_2$ ($X=\text{Cl}$ and Br). Magnetic refinement parameters determined from the A-bank of POLARIS for $\text{Sr}_2\text{CoO}_2\text{Cl}_2$ (20 K) and $\text{Sr}_2\text{CoO}_2\text{Br}_2$ (2 K) are also shown. The * represents reflection contaminated by nuclear intensity.

(h, k, l)	$\text{Sr}_2\text{CoO}_2\text{Cl}_2$				Observed intensity	$\text{Sr}_2\text{CoO}_2\text{Br}_2$		Observed intensity
	Model I La_2CuO_4	Model II La_2NiO_4	Model III K_2NiF_4	Model I+II		Model III K_2NiF_4	Model I+II	
(100)	3.81	0	4.74	3.93	4.65(4)	3.46	1.62	1.85(3)
(011)	0.59	4.69	6.66	5.16	5.33(3)	5.07	4.40	4.25(4)
(102)	2.37	1.05	2.65	3.28	3.25(3)	2.25	2.05	2.12(2)
(013)	0.65	1.51	0.88	2.12	2.05(3)	0.86	2.39	2.36(3)
(104)	0.59	0.59	0.27	1.03	8.45(2)*	0.33	0.87	0.96(3)
	$ \mu (\mu_B)$		3.22(4)				3.52(7)	
	Model I: Model II (%)		48(1):52(1)				34(1):66(1)	
	R_{wp} (%)		3.64				2.63	
	R_p (%)		4.69				2.97	
	χ^2		0.88				1.11	

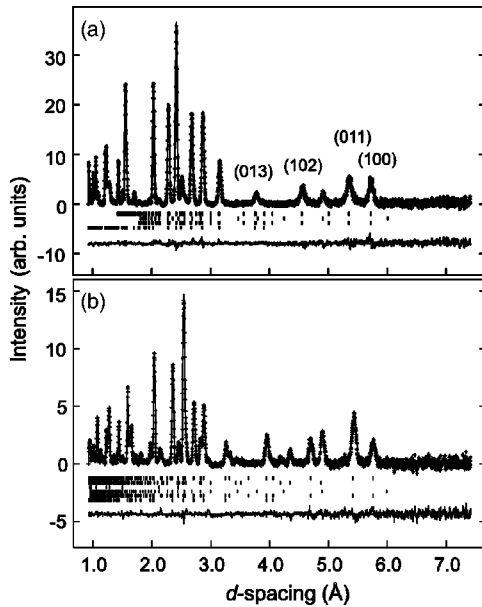


FIG. 3. The NPD pattern obtained for $\text{Sr}_2\text{CoO}_2\text{Cl}_2$ (a) and $\text{Sr}_2\text{CoO}_2\text{Br}_2$ (b) at 20 K and 2 K, respectively. The plot follows the same labeling style as in Fig. 2. In (a) tick marks indicate, from bottom to top, the nuclear structure of $\text{Sr}_2\text{CoO}_2\text{Cl}_2$, the La_2CuO_4 -type magnetic phase, the magnetic structure of CoO and the La_2NiO_4 -type magnetic phase. Also marked are the most intense $\text{Sr}_2\text{CoO}_2\text{Cl}_2$ magnetic reflections. In (b) contributions from $\text{Sr}_2\text{CoO}_2\text{Br}_2$ (nuclear), $\text{Sr}_2\text{CoO}_2\text{Br}_2$ (La_2CuO_4 magnetic), CoO (nuclear and magnetic), SrCO_3 and $\text{Sr}_2\text{CoO}_2\text{Br}_2$ (La_2NiO_4 magnetic) are shown reading from bottom to top.

for the doubling of the magnetic cell) before being permitted to vary. This produced little deviation from the initial phase distribution for the $\text{Sr}_2\text{CoO}_2\text{Cl}_2$ refinement, i.e., the refined phase fractions were 48(1):52(1) indicating the coexistence of approximately equal numbers of La_2CuO_4 -type and La_2NiO_4 -type domains within the material. In contrast the $\text{Sr}_2\text{CoO}_2\text{Br}_2$ analysis revealed a 34(1):66(1) preference for the La_2NiO_4 spin arrangement. Analysis of $\text{Sr}_2\text{CoO}_2\text{Cl}_2$ data sets collected at higher temperatures revealed that the magnetic phase ratio remained constant on warming. Table II summarizes the observed and calculated magnetic intensity obtained for the trial magnetic structures for both materials and also presents details of the magnetic refinements.

In addition to the magnetic reflections from $\text{Sr}_2\text{CoO}_2\text{Cl}_2$ and $\text{Sr}_2\text{CoO}_2\text{Br}_2$ a peak at ~ 4.9 Å was identified as the (111) magnetic reflection of the CoO impurity present in both samples and was fitted using the model of Roth.²¹ The final agreement achieved to the A-bank diffraction profiles of $\text{Sr}_2\text{CoO}_2\text{Cl}_2$ and $\text{Sr}_2\text{CoO}_2\text{Br}_2$ is shown in Fig. 3.

IV. DISCUSSION

The $\text{Sr}_2\text{CoO}_2\text{X}_2$ materials both undergo a transition to AF long range order below room temperature. Susceptibility (χ) data obtained for $\text{Sr}_2\text{CoO}_2\text{Cl}_2$ (Ref. 16) revealed a drop in χ on cooling from 320 K to ≈ 200 K, strongly suggesting the presence of AF interactions between the Co spins and the transition to a 3D long-range ordered state is consistent with

these results. The magnetic intensities observed for both $\text{Sr}_2\text{CoO}_2\text{Cl}_2$ and $\text{Sr}_2\text{CoO}_2\text{Br}_2$ can be explained by the coexistence of two closely related collinear magnetic phases, the La_2CuO_4 and La_2NiO_4 spin arrangements shown in Fig. 1. The structures differ only in the relative orientation of the interlayer nearest neighbors, which may be rotated by 180° to transform from one to another. The exact reasons for the observed spin anisotropy within lamellar antiferromagnets remain a topic of considerable interest.²² Generally the onset of 3D order within planar antiferromagnets is considered to involve an xy anisotropy above T_N that confines the spins to the basal plane and a separate Ising anisotropy determines the in-plane spin direction.²³ The crossover to 3D long range order then requires the presence of an interlayer interaction that becomes increasingly significant as the 2D correlation length grows. Given that the La_2CuO_4 and La_2NiO_4 spin structures both possess two ferromagnetic and two antiferromagnetic nearest neighbors in the planes above and below any energy difference between the configurations is likely to be small. Consequently the most likely explanation for the coexistence of the two spin structure domains within the cobalt oxyhalides is the presence of two distinct interlayer interactions that determine the relative stacking of the AF sheets. In this context the refinement of the parameters for the chloride and bromide ions (Table I) indicative of structural disorder within the SrX rocksalt layers is significant as the interlayer exchange coupling will be mediated through these bonds. Localized variations in these pathways could lead to different interlayer interactions and stabilize one spin structure in a particular region of the material. Similarly, crystal defects such as stacking faults may also alter the exchange between the CoO_2 sheets.

Another factor that may promote the growth of different magnetic structure domains is a level of sample inhomogeneity, which given the presence of small levels of impurities in both the polycrystalline samples used in this study is a possibility. Nevertheless, even in single crystals it is not so unusual for two magnetic phases to coexist as demonstrated by Rb_2MnF_4 .⁹ In fact the presence of both La_2CuO_4 and La_2NiO_4 type domains has previously been suggested by Matsuda *et al.* in a study of Nd_2CuO_4 .²⁴ Their single crystal was found to undergo a magnetic phase transition from the La_2NiO_4 to La_2CuO_4 structure similar to that of La_2CoO_4 ,⁸ however a level of the nickelate spin lattice appears to persist below the transition temperature emphasizing the near degeneracy of the two spin configurations.

The magnetic reflections of $\text{Sr}_2\text{CoO}_2\text{Cl}_2$ [Fig. 4(a)] became indistinguishable from the background on heating from 195 K to 220 K allowing the material's $T_N = 215 \pm 10$ K to be estimated. The relative intensity of the magnetic peaks remains constant within experimental uncertainty indicating that the transition temperatures for both magnetic phases within $\text{Sr}_2\text{CoO}_2\text{Cl}_2$ are likely to be very similar, and also therefore, that the strength of the interlayer interactions are closely matched. The uniform growth of the peaks is also consistent with the absence of any spin reorientations within the domains below the transition. The onset of long range order occurs approximately 40 K lower than the Néel temperatures typically reported for $\text{Sr}_2\text{CuO}_2\text{Cl}_2$, a relatively small difference which indicates that the strength of the ex-

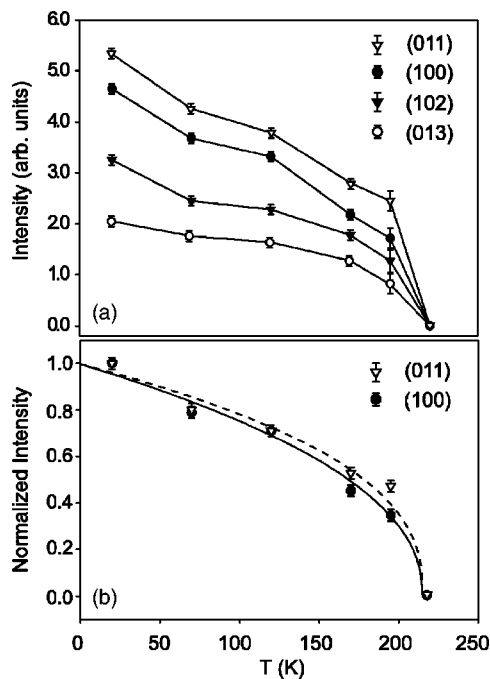


FIG. 4. The temperature dependence of the integrated intensity of the most intense magnetic reflections observed for $\text{Sr}_2\text{CoO}_2\text{Cl}_2$ (a). The normalized intensity of the (100) and (011) peaks is shown in (b) along with fits to the power law $A(1-T/T_N)^\beta$.

change interactions lies on a similar energy scale to that found in the cuprates. The transition temperature is somewhat lower than the T_N of 275 K determined for La_2CoO_4 (Ref. 8) and follows the trend of a decrease in the Néel temperature observed for the analogous oxychloride and oxide cuprates, i.e., $\text{Sr}_2\text{CuO}_2\text{Cl}_2$, $T_N=251$ K and La_2CuO_4 , $T_N=325$ K.^{11,25} The origin of this reduction most probably lies in the expanded metal to metal distances found in the oxyhalides, both within the metal oxygen planes and across the separating layers, which is expected to weaken orbital overlap and the strength of exchange coupling. The structural change that occurs in the halide containing phases is perhaps best illustrated by considering the nearest neighbor distance between the planes. This increases from ~ 7.1 Å in La_2CuO_4 to 8.3 Å in $\text{Sr}_2\text{CuO}_2\text{Cl}_2$ (Ref. 11) and similarly from 6.85 Å in La_2CoO_4 (Ref. 26) to 8.01 Å in $\text{Sr}_2\text{CoO}_2\text{Cl}_2$. Alternatively it has been suggested that the approximate 20% reduction in T_N typically observed for tetragonal phases such as Pr_2CuO_4 and Sm_2CuO_4 in comparison with orthorhombic La_2CuO_4 results due to the inherent frustration of the interlayer coupling within the higher symmetry systems²⁷ and similar effects may also play a role in $\text{Sr}_2\text{CuO}_2\text{Cl}_2$ and $\text{Sr}_2\text{CoO}_2\text{Cl}_2$.

The development of the sublattice magnetization is shown in Fig. 4(b), which plots the normalized intensity of the (100) and (011) reflections. Also shown are the fits achieved to a simple power law of the form $A(1-T/T_N)^\beta$ over the entire, ~ 200 K, temperature range with $A=0.99(1)$, $T_N=215$ K, and exponent $\beta=0.45(4)$ for the (100) reflection (solid line) and $\beta=0.39(5)$ for the (011) peak (broken line). The growth of the (100) reflection reflects solely the behavior of the La_2CuO_4 -type domains, while the (011) peak contains inten-

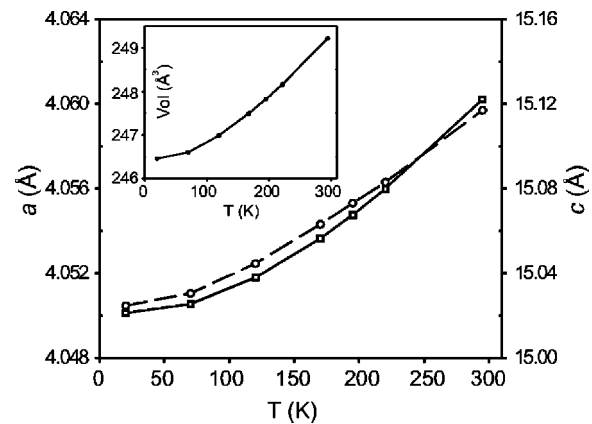


FIG. 5. Temperature dependence of the lattice constants a (square symbols) and c (circles) of $\text{Sr}_2\text{CoO}_2\text{Cl}_2$. Inset shows the thermal behavior of the unit cell volume.

sity contributions from both La_2CuO_4 and La_2NiO_4 spin structures. The similarity of the β values therefore provides additional support for a single, or at least extremely close, transition temperature for the magnetic domains. The absence of further data close to the ordering temperature prevents us from determining precisely the exponent of the magnetic phase transition in the critical region. However, the β values are significantly larger than those determined for classical Ising-type 2D systems such as K_2NiF_4 in which a $\beta \approx 0.15$ provides a good fit to the whole experimental data range.⁹ The values also contrast strongly with the critical behavior of La_2CoO_4 for which $\beta=0.20$.⁸ In fact the derived exponents lie closer to that determined for $\text{Sr}_2\text{CuO}_2\text{Cl}_2$, $\beta=0.30 \pm 0.02$,¹¹ and are indicative of 3D transitions for which $\beta \approx 0.33$. Physically the relevance of this is to suggest that interlayer coupling is of greater importance within the materials in comparison to the behavior of K_2NiF_4 in which long range magnetic order is established essentially in two dimensions.

In common with $\text{Sr}_2\text{CuO}_2\text{Cl}_2$ our NPD refinements reveal no evidence for a structural phase transition in either $\text{Sr}_2\text{CoO}_2\text{Cl}_2$ or $\text{Sr}_2\text{CoO}_2\text{Br}_2$ and the materials average crystal structures is satisfactorily modeled in tetragonal symmetry over the measured temperature range. Strictly, the symmetry of the systems must be reduced from tetragonal to orthorhombic at the onset of long range magnetic order as may be seen by considering the La_2CuO_4 and La_2NiO_4 spin structures shown in Fig. 1, but the distortion clearly lies below the resolution limits of our current study. The importance of this small deviation from tetragonal symmetry is to relieve the frustration associated with the otherwise identical interlayer exchange pathways in the materials. The temperature dependence of the cell parameters and cell volume, shown in Fig. 5, reveals a smooth thermal expansion that is also apparent in the basal Co-O, and apical Co-Cl interatomic distances presented in Fig. 6. In contrast to our recent investigation of the closely related cobalt (III) oxychloride $\text{Sr}_2\text{CoO}_3\text{Cl}$,²⁸ the data reveal no evidence of any structural anomalies associated with the onset of long range order. The absence of significant crystal structure distortions is a key difference between the $\text{Sr}_2\text{MO}_2\text{X}_2$ oxyhalide and La_2MO_4 ($M=\text{Cu}$ and Co) oxide

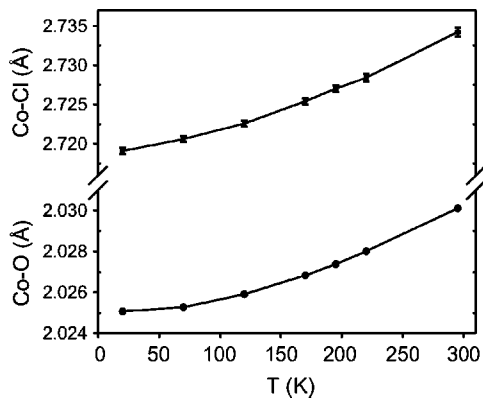


FIG. 6. Thermal evolution of the basal Co-O and apical Co-Cl distances of $\text{Sr}_2\text{CoO}_2\text{Cl}_2$.

systems. As mentioned above incorporation of the larger chloride and bromide ions in the separating rocksalt layers above and below the MO_2 planes produces a significantly expanded metal environment. For example, the planar Co-O distance in $\text{Sr}_2\text{CoO}_2\text{Cl}_2$ is 2.030 Å compared with 1.944 Å in La_2CoO_4 .²⁶ Consequently the compressive bond strain that drives the various rotations and tilts displayed by the MO_6 octahedra in the equivalent oxides is alleviated. These relatively small departures from the ideal K_2NiF_4 symmetry often have important implications for the magnetism displayed by the oxides as exemplified by the spin rearrangement of La_2CoO_4 and the ferromagnetic moment exhibited by La_2CuO_4 .²⁹

The moments for $\text{Sr}_2\text{CoO}_2\text{Cl}_2$ and $\text{Sr}_2\text{CoO}_2\text{Br}_2$ at 20 K and 2 K are, respectively, $3.22(4)\mu_B$ and $3.52(7)\mu_B$. To obtain these values it was assumed that the magnitude of the moment within the two magnetic phases would be the same. This seems plausible given that the strength of the intralayer coupling will be identical within the two spin structures, and the interlayer interactions are also likely to be very closely matched as discussed previously. The refined moments are both larger than the spin only value of $3\mu_B$ expected for high spin Co^{2+} ($S=3/2$) and suggest a significant orbital contribution to the ordered moment, particularly as the magnitude of the refined moment is expected to be reduced somewhat from its ideal value due to fluctuations within the AF sheets. A sizeable orbital component is commonly observed for the Co^{2+} ion, with, for example, a recent study on CoO reporting a moment of $3.98(6)\mu_B$.³⁰

The static moments are higher than the $2.9 \pm 0.1\mu_B$ obtained by Yamada *et al.*⁸ for their single crystal of La_2CoO_4 . Possibly this reflects the presence of a weaker crystal field in the oxyhalide phases and hence a larger (unquenched) orbital contribution to the moment in the $\text{Sr}_2\text{CoO}_2\text{X}_2$ phases. It is worth noting that the increased magnitude of the moments for the Co oxyhalide systems in comparison to the values of $\sim 0.2\text{--}0.4\mu_B$ typically reported for layered cuprates greatly aid the observation of magnetic Bragg reflections for the former materials in our powder samples and will also facilitate future studies on single crystals.

Finally, it is informative to compare in more detail the behavior of the $\text{Sr}_2\text{CoO}_2\text{X}_2$ ($X=\text{Cl}, \text{Br}$) materials with those recently reported for another single layer cobalt oxychloride,

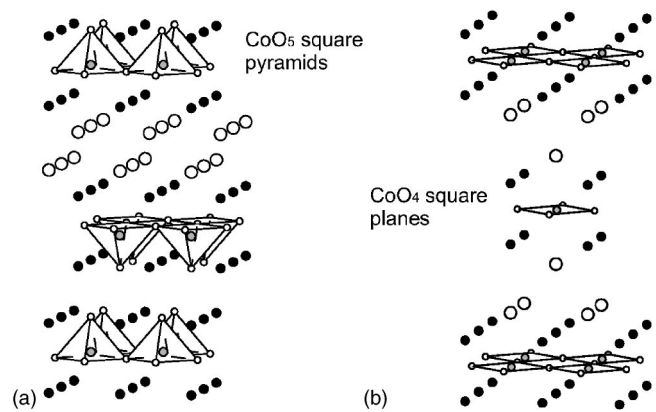


FIG. 7. Crystal structures of $\text{Sr}_2\text{CoO}_3\text{Cl}$ (a) and $\text{Sr}_2\text{CoO}_2\text{Cl}_2$ (b) showing the differing cobalt to oxygen coordination in the materials. Large open spheres represent chloride ions, medium shaded spheres represent cobalt, medium black spheres represent strontium, and small open spheres represent oxygen.

$\text{Sr}_2\text{CoO}_3\text{Cl}$.²⁸ These systems provide a good illustration of the flexibility of oxyhalide systems with the cobalt valence state changing from +2 in $\text{Sr}_2\text{CoO}_2\text{X}_2$ to +3 in $\text{Sr}_2\text{CoO}_3\text{Cl}$ as a function of the halide to oxide ratio. Structurally the impact of the sequentially replacing the apical oxide ions by chloride within the currently unknown K_2NiF_4 phase Sr_2CoO_4 is to change the cobalt coordination from octahedral to distorted square pyramidal in $\text{Sr}_2\text{CoO}_3\text{Cl}$ through to square planar in $\text{Sr}_2\text{CoO}_2\text{Cl}_2$ (see Fig. 7). While the structures are closely related, ordering of the single chloride ion per formula unit within $\text{Sr}_2\text{CoO}_3\text{Cl}$ removes the body centering normally associated with K_2NiF_4 -type materials. Comparison of the observed room temperature bond lengths reflects the higher cobalt oxidation state of $\text{Sr}_2\text{CoO}_3\text{Cl}$, which possesses an in-plane Co-O bond close to 1.97 Å, approximately 0.06 Å shorter than those found in $\text{Sr}_2\text{CoO}_2\text{Cl}_2$. The material undergoes a transition to an AF long range ordered state with a $T_N=330(5)$ K, approximately 100 K higher than that of $\text{Sr}_2\text{CoO}_2\text{Cl}_2$, and adopts a La_2NiO_4 -type spin structure. Within both materials the dominant superexchange interactions will be mediated through the half-occupied cobalt $d_{x^2-y^2}$ and the oxygen p_x, p_y orbitals and it is therefore tempting to conclude that the significantly shorter Co-O in-plane distance exhibited by $\text{Sr}_2\text{CoO}_3\text{Cl}$ leads to increased overlap and the observed strengthening in coupling. However such a simple interpretation is complicated by the significant ($\sim 20^\circ$) buckling of the basal CoO_2 plane found in $\text{Sr}_2\text{CoO}_3\text{Cl}$ that is expected to weaken both effective overlap and the strength of the exchange interaction. At a first approximation it seems the reduced separation of the ions is more important than the bond angle in governing the strength of the magnetism in these phases although the differing interlayer pathways are also likely to play a role in determining the 3D transition temperatures. In contrast to $\text{Sr}_2\text{CoO}_2\text{Cl}_2$ the transition to long range order in $\text{Sr}_2\text{CoO}_3\text{Cl}$ is preceded by the presence of significant diffuse magnetic scattering arising from extended regions of 2D spin correlation. Peculiarly the diffuse feature persists well below T_N due, it is believed, to stacking faults within the sample investigated. Finally, the

size of the moment obtained at 2 K, $2.82(3)\mu_B$, is smaller than those obtained for the $\text{Sr}_2\text{CoO}_2\text{X}_2$ counterparts. This runs contrary to the expected behavior of high spin d^6 ($S=2$) and high spin d^7 ($S=3/2$) systems. It is possible that a greater orbital contribution within the $\text{Sr}_2\text{CoO}_2\text{X}_2$ materials is responsible for this discrepancy. Alternatively the refined moment of $\text{Sr}_2\text{CoO}_3\text{Cl}$ may be reduced considerably by either the static stacking disorder found in the material or enhanced covalency.

In summary we have used NPD to determine the presence of antiferromagnetic order within the square lattice Co(II) phases $\text{Sr}_2\text{CoO}_2\text{Cl}_2$ and $\text{Sr}_2\text{CoO}_2\text{Br}_2$. Like the isostructural cuprate $\text{Sr}_2\text{CuO}_2\text{Cl}_2$ the cobalt phases retain an average tetragonal crystal structure in the AF ordered state. The magnitude of the refined moments indicates that cobalt is present in a high spin state and the observed magnetic scattering is

consistent with antiferromagnetic near neighbor in-plane Co to Co coupling. However two distinct interlayer nearest neighbor spin orientations, corresponding to the La_2CuO_4 and La_2NiO_4 spin arrangements, are required to account for the observed intensity. Further investigations on predominantly single domain crystals are required to clarify which of these spin structures is the true ground state of the materials.

ACKNOWLEDGMENTS

The authors acknowledge the technical assistance of Dr. Ron Smith of the ISIS facility. We also thank Dr. Daniel Price, University of Southampton, and Dr. Andrew Wills, University College London, for helpful discussions relating to magnetism and magnetic diffraction. This work has been supported by the EPSRC through Grant No. GR/R99591/01.

*Author to whom correspondence should be addressed. Present address: Department of Applied Physics, Chalmers University of Technology, SE-412 96 Gothenburg, Sweden. Email address: knee@fy.chalmers.se

¹R.J. Cava, R.B. van Dover, B. Batlogg, and E.A. Rietman, *Phys. Rev. Lett.* **58**, 408 (1987).

²J.E. Greedan, A.H. O'Reilly, and C.V. Stager, *Phys. Rev. B* **35**, 8770 (1987).

³D. Vaknin, S.K. Sinha, D.E. Moncton, D.C. Johnston, J.M. Newsam, C.R. Safinya, and H.E. King, Jr., *Phys. Rev. Lett.* **58**, 2802 (1987).

⁴M.C. Aronson, S.B. Dierker, B.S. Dennis, S.W. Cheong, and Z. Fisk, *Phys. Rev. B* **44**, 4657 (1991).

⁵E. Manousakis, *Rev. Mod. Phys.* **63**, 1 (1991).

⁶G. Aeppli and D.J. Buttrey, *Phys. Rev. Lett.* **61**, 203 (1988).

⁷K. Nakajima, K. Yamada, S. Hosoya, T. Omata, and Y. Endoh, *J. Phys. Soc. Jpn.* **62**, 4438 (1993).

⁸K. Yamada, M. Matsuda, Y. Endoh, B. Keimer, R.J. Birgeneau, S. Onodera, J. Mizusaki, T. Matsuura, and G. Shirane, *Phys. Rev. B* **39**, 2336 (1989).

⁹R.J. Birgeneau, H.J. Guggenheim, and G. Shirane, *Phys. Rev. B* **1**, 2211 (1970).

¹⁰E.J. Samuelsen, *Phys. Rev. Lett.* **31**, 936 (1973).

¹¹D. Vaknin, S.K. Sinha, C. Stassis, L.L. Miller, and D.C. Johnston, *Phys. Rev. B* **41**, 1926 (1990).

¹²F. Borsa, M. Corti, T. Goto, A. Rigamonti, D.C. Johnston, and F.C. Chou, *Phys. Rev. B* **45**, 5756 (1992).

¹³Y.J. Kim, R.J. Birgeneau, F.C. Chou, R.W. Erwin, and M.A. Kastner, *Phys. Rev. Lett.* **86**, 3144 (2001).

¹⁴G. Blumberg, P. Abbamonte, M.V. Klein, W.C. Lee, D.M. Ginsberg, L.L. Miller, and A. Zibold, *Phys. Rev. B* **53**,

R11 930 (1996).

¹⁵C.S. Knee and M.T. Weller, *J. Mater. Chem.* **13**, 1507 (2003).

¹⁶C.S. Knee and M.T. Weller, *J. Solid State Chem.* **168**, 1 (2002).

¹⁷H.M. Rietveld, *J. Appl. Crystallogr.* **2**, 65 (1969).

¹⁸A.C. Larson and R.B. von Dreele, *General Structure Analysis System* (Los Alamos National Laboratory, Los Alamos, 1994).

¹⁹P.J. Brown, *International Tables for Crystallography* (Kluwer Academic, Dordrecht, 1992), Vol. C, p. 391.

²⁰A.S. Wills, *Physica B* **276**, 680 (2000), program available from <ftp://ill.fr/pub/dif/sarah>

²¹W.L. Roth, *Phys. Rev.* **110**, 1333 (1958).

²²T. Yildirim, A.B. Harris, O. Entin-Wohlman, and A. Aharony, *Phys. Rev. Lett.* **72**, 3710 (1994), and references therein.

²³D. Vaknin, L.L. Miller, and J.L. Zarestky, *Phys. Rev. B* **56**, 8351 (1997).

²⁴M. Matsuda, K. Yamada, K. Kakurai, H. Kadowaki, T.R. Thurston, Y. Endoh, Y. Hidaka, R.J. Birgeneau, M.A. Kastner, P.M. Gehring, A.H. Moudden, and G. Shirane, *Phys. Rev. B* **42**, 10 098 (1990).

²⁵B. Keimer, A. Aharony, A. Auerbach, R.J. Birgeneau, A. Casanholo, Y. Endoh, R.W. Erwin, M.A. Kastner, and G. Shirane, *Phys. Rev. B* **45**, 7430 (1992).

²⁶U. Lehmann and H. Müller-Buschbaum, *Z. Anorg. Allg. Chem.* **470**, 59 (1980).

²⁷M.A. Kastner, R.J. Birgeneau, G. Shirane, and Y. Endoh, *Rev. Mod. Phys.* **70**, 897 (1998).

²⁸C.S. Knee, D.J. Price, M.R. Lees, and M.T. Weller, *Phys. Rev. B* **68**, 174407 (2003).

²⁹T. Thio and A. Aharony, *Phys. Rev. Lett.* **73**, 894 (1994).

³⁰W. Jauch, M. Reehuis, H.J. Bleif, F. Kubanek, and P. Pattison, *Phys. Rev. B* **64**, 052102 (2001).